ARCHIVES OF ELECTRICAL ENGINEERING VOL. 67(4), pp. 899–913 (2018)

DOI 10.24425/aee.2018.124748

Research on the operational performance of high speed permanent magnet generator with controlled rectifier in distributed generation

QIU HONGBO, WEI YANQI, YANG CUNXIANG, HU KAIQIANG

School of Electrical and Information Engineering, Zhengzhou University of Light Industry
Zhengzhou, Henan, China
e-mail: weiyanqi92@163.com

(Received: 24.06.2018, revised: 11.09.2018)

Abstract: The uncontrolled rectifier and controlled rectifier which use fixed switching frequency control strategy are applied usually during the working of a high-power high-speed permanent magnet generator (HSPMG). Even for the controlled rectifier, it will generate harmonics. The electromagnetic performance of the HSPMG is also affected by these harmonics. In this paper, the influences of the fixed switching frequency control strategy on a HSPMG were studied. Based on the Fourier theory, the harmonic currents of the generator were analyzed, and the change of harmonic distribution range and current total harmonic distortion (THD) were obtained. By using an indirect field-circuit coupling method, the influences of the fixed switching frequency control strategy on the losses and torque of the generator were analyzed. The relations between the switching frequency and the losses and torque of the generator were obtained, and the change mechanism of the loss was revealed. The obtained conclusions can provide reference for the optimized choice of the switching frequency of the distributed generation system with the HSPMG. It can also provide support for the HSPMG electromagnetic structural optimization and the optimization of the loss and harmonic on the system level.

Key words: high speed permanent magnet generator, controlled rectifier, electromagnetic field, switching frequency

1. Introduction

The distributed generation which is based on HSPMG driven by a micro gas turbine has not only small size, little noise and high power density of HSPMG, but also high efficiency, little pollution, simple structure, low construction and maintenance costs of the micro gas turbine system [1–3]. The distributed generation can also improve the reliability and efficiency of the power system. So it has a wide range of application and receives extensive attention.

The speed of the HSPMG can reach tens of thousands of revolutions per minute in the normal state, and the frequency of the output electric energy is thousands of Hertz, in general [4–5]. The rectifier is necessary in this kind of distributed generation. Both uncontrolled and controlled rectifiers are nonlinear devices, which will lead to the system that has a large amount of a harmonic current on an AC side. The harmonic will cause a lot of harm to the HSPMG. The effects of an uncontrolled rectifier on the electromagnetic field and temperature field of the HSPMG were studied, and some useful conclusions are obtained to optimize the HSPMG in References [6–7]. The influences of the driving circuit switching frequency on the losses of windings and magnets were analyzed, and some useful conclusions were obtained in Reference [8]. But the analysis of other permanent magnet motor operation performance and the optimization of switching frequency were not involved. The influence of switch control strategy on the permanent magnet motor core loss was studied in References [9–12]. The analysis of high speed permanent magnet motor loss was investigated under different control strategies in References [13–16], and the advantages and disadvantages of different control strategies are discussed. Though some researchers studied the influence of the control strategy on a high speed permanent magnet motor, these studies only focused on the losses of a low-power motor. And the study on the influence of rectifier switching frequency on the operation performance of a high-power high-speed permanent magnet generator is few, the study of its influence mechanism is fewer.

In this paper, taking an HSPMG driven by a micro gas turbine as an example, based on the theory of motor transient analysis and the Fourier theory, the influence of the different rectifier switching frequency on the generator harmonic current is analyzed. Since the direct field-circuit coupling method is very time-consuming, the indirect field-circuit coupling method is used to analyze the influences of the different switching frequency control strategy of a rectifier on the electromagnetic field of the generator in this paper [17]. Its influence mechanisms are revealed, and some useful conclusions are obtained. These conclusions not only can provide a useful reference and theoretical basis for the switching frequency selection of the rectifier in the distributed generation system, but also can provide reference for the optimization of the HSPMG, as well as the system level harmonic optimization and loss optimization to prevent a demagnetization fault.

2. Models in the analysis process

The studied object in this paper is an HSPMG. The back winding structure is used to shorten the length of the stator end windings for a stator armature winding, as shown in Fig. 1 [18]. The generator cooling system is the closed oil cooling system. The stator slots and back windings space are cooled by oil, and oil filling rings are placed in the air gap. Sleeve material is made of austenitic retaining ring steel (50Mn18Cr5). The permanent magnet (PM) is SM-26U. The PM has a remanence (Br) temperature coefficient of -0.03% K^{-1}, and the electrical conductivity is 1.2×10^6 S/m [6]. A sectional ring type is used as the magnetic pole structure. The basic parameters of the HSPMG are shown in Table 1.

Table 1. Basic parameters of the HSPMG

Parameter name	Value	Unit	Parameter name	Value	Unit
Rated power	117	kW	Sleeve thickness	5.5	mm
Rated voltage	670	V	Single conductor diameter	0.63	mm
Rated frequency	1	kHz	Stator outer diameter	135	mm
Rotor type	PM		Stator inner diameter	72	mm
Pole number	2		Rotor outer diameter	66	mm
Permanent magnet number	12		Core length	275	mm
Parallel branch number	1		Slot number	36	

2.1. The 2D finite element model of the generator

The 2D finite element model (FEM) is established according to the structure size and parameter of the generator prototype to analysis the influence of the time harmonic current on a generator electromagnetic field, as shown in the Fig. 1.

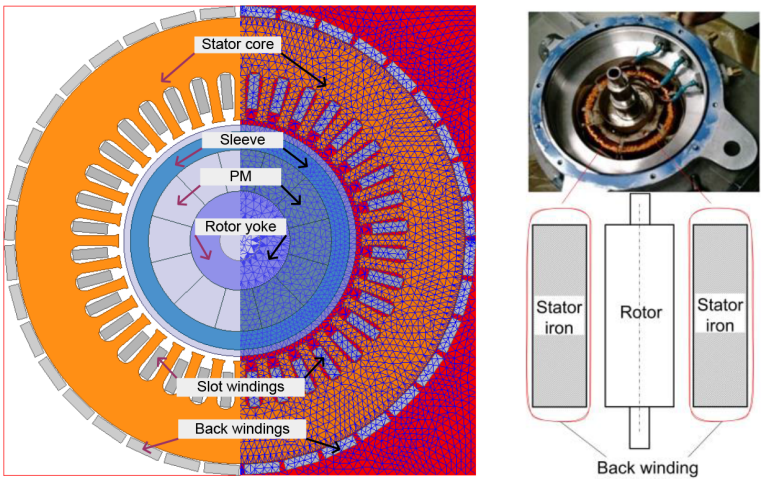

(a) (b)

Fig. 1. The generator: (a) the 2D finite element model; (b) the backing winding structure

In order to simplify the analysis and calculation of the electromagnetic fields, the following assumptions are applied:

a. The influence of a displacement current is ignored, and the electromagnetic field in the generator is a quasi-stationary electromagnetic field.
b. The magnetic vector potential has only Z-axis components during the 2D transient field analysis.
c. Materials are isotropic. The permeability of the material is constant and the variation of the permeability with the change of the temperature is ignored [5].

Based on the above assumptions and electromagnetic field theory, the boundary value equations of the generator 2D transient electromagnetic field are presented as Formula (1) [5]:

$$\begin{cases} \dfrac{\partial}{\partial x}\left(\dfrac{1}{\mu}\dfrac{\partial A_z}{\partial x}\right)+\dfrac{\partial}{\partial y}\left(\dfrac{1}{\mu}\dfrac{\partial A_z}{\partial y}\right)=-\left(J_z-\sigma\dfrac{\mathrm{d}A_z}{\mathrm{d}t}\right) \\ A_z=0 \\ \dfrac{1}{\mu_1}\dfrac{\partial A_z}{\partial n}-\dfrac{1}{\mu_2}\dfrac{\partial A_z}{\partial n}=J_s \end{cases}, \tag{1}$$

where A_z is the magnetic vector potential, J_z is the conduction current density, μ is the magnetic permeability, σ is the conductivity, J_s is the equivalent current density of the permanent magnet, t is the time, n is the normal direction of the permanent magnet boundary.

2.2. The state-space model of the generator

Based on the theory of motor transient analysis, in order to analyse the harmonic current generated by the rectifier with different switching frequency control strategy, the generator mathematical model (based on d-q coordinate system) is built, as Formula (2) [19]. The block diagram is shown in Fig. 3.

$$\begin{cases} \dfrac{\mathrm{d}i_d}{\mathrm{d}t}=\dfrac{L_q i_q \omega_r p}{L_d}-\dfrac{U_d}{L_d}-\dfrac{R_a i_d}{L_d} \\ \dfrac{\mathrm{d}i_q}{\mathrm{d}t}=\dfrac{\psi_f \omega_r p}{L_q}-\dfrac{U_q}{L_q}-\dfrac{L_d i_d \omega_r p}{L_q}-\dfrac{R_a i_q}{L_q} \\ T_e=\dfrac{3i_q p}{2}\left(\psi_f-L_d i_d+L_q i_d\right) \end{cases}, \tag{2}$$

where U_d, U_q are the direct-axis and quadrature-axis stator voltages, i_d, i_q are the direct-axis and quadrature-axis stator currents, L_d, L_q represent the direct-axis and quadrature-axis synchronous inductance, R_a is the armature resistance, ω_r is the mechanical angular velocity, p is the pole-pair number of the generator, ψ_f is the flux linkage of the PM.

2.3. Experimental study of the generator

The accuracy of the established finite element model and the state-space model is verified by the test of the generator prototype.

First of all, the terminal voltage and armature current of the generator operating at different speeds (including 6 000 rpm, 8 000 rpm and 10 000 rpm) under the same load are tested. After that, the terminal voltage and armature current are obtained from the finite element model and the state-space model. Finally, through comparing and analyzing the three sets of results, the accuracy of these two models was verified.

The experimental platform and the experimental equipment are shown in Fig. 2.

After testing the prototype and calculating the two models, the test results of the generator and the calculation results of the finite element model and the state-space model are shown in Table 2.

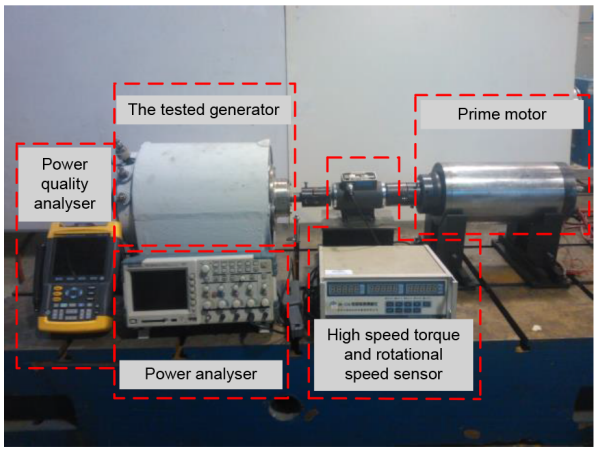

Fig. 2. The test platform

Table 2. Comparisons of the test data of the prototype and the calculation data of different models

Speed (rpm)		**6 000**	**8 000**	**10 000**
Test result	terminal voltage (V)	39.6	53.7	65.1
	armature current (A)	14.4	18.5	22.1
Calculation results of finite element model	terminal voltage (V)	39.9	53.1	65.8
	armature current (A)	14.5	18.3	22.4
Calculation results of state-space model	terminal voltage (V)	39.6	52.8	65.9
	armature current (A)	14.4	18.2	22.4

Through comparison and analysis, it becomes clear that the errors between the two models and the prototype are less than 1.7%, which falls within the allowable error range. Therefore, the three sets of data could be considered consistent. The established finite element model and the state-space model are accurate.

3. Harmonic of HSPMG with SPWM controlled rectifier

Recently, since the social production is becoming more and more demanding for the quality and safety of energy and power supply, small-scale and decentralized distributed generation systems have been developed rapidly to make up for the shortage of a large power grid. The HSPMG driven by a micro gas turbine has many advantages, and it plays a very important role in a distributed generation system. Since the frequency of the HSPMG output power is above 1 kHz, the output power can't be directly used by ordinary AC users. So in order to convert high-frequency AC to DC, the rectifier is necessary. In this paper, in order to analyzing the influence of multi frequency coupling harmonics of the different rectifier switching frequency on the HSPMG

and the distributed generation system, the dynamic analysis model of the rectification system is built based on the dynamic coupling circuit method. The block diagram is shown in Fig. 3.

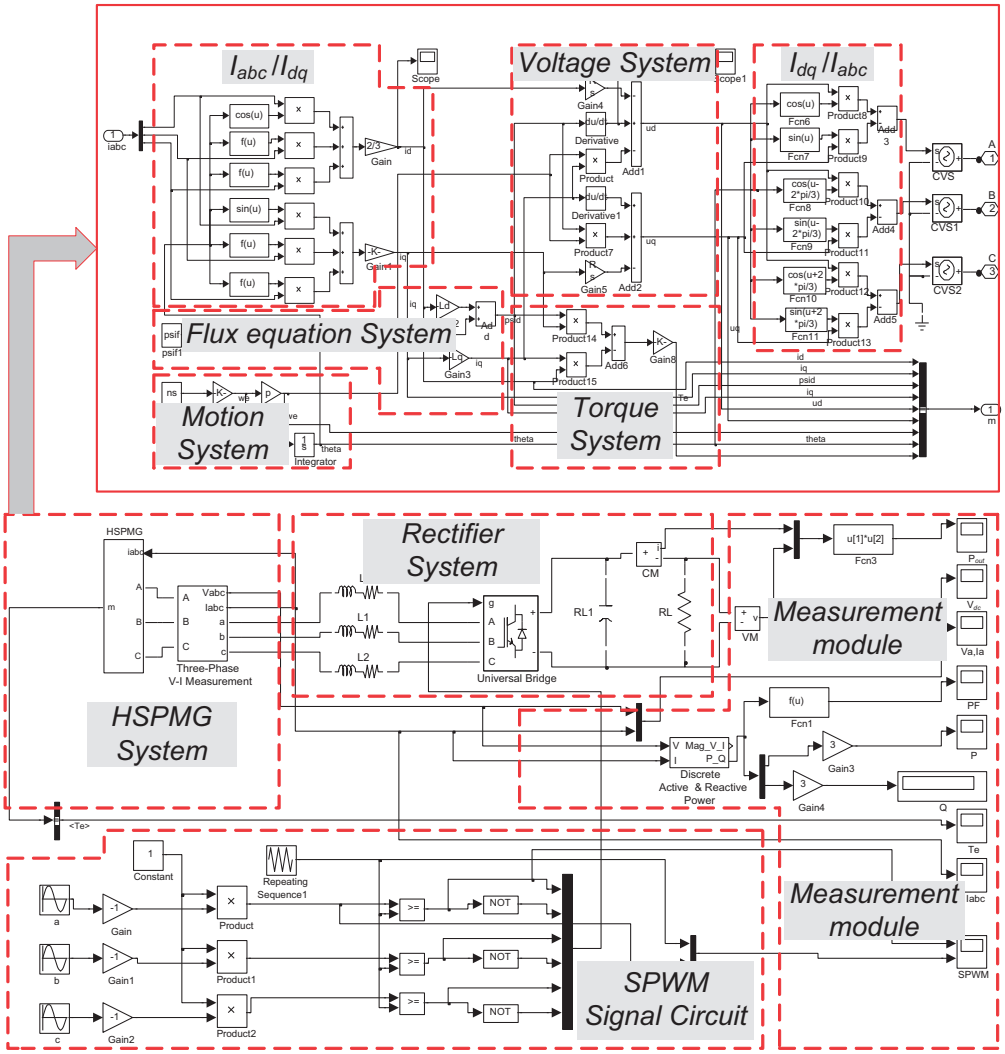

Fig. 3. The block diagram of the state-space model

During the research, in order to facilitate the analysis and calculation, the output power of the generator is rated power, and the power factor is 0.91.

3.1. Phase current harmonic of the system

In this paper, the switching frequency which is 3 times (6, 9, 12,. . .) of the fundamental frequency, is adopted to ensure three-phase current balance. When the switching frequency

which is 3 odd times of the fundamental frequency is adopted, the harmonic orders are odd times. When 3 even times of the fundamental frequency are adopted as the switching frequency, the harmonic orders are odd times and even times. The output SPWM waveforms are shown in Fig. 4 when the carrier ratio (the ratio of the switching frequency to the fundamental frequency) is 3 odd times and 3 even times, respectively.

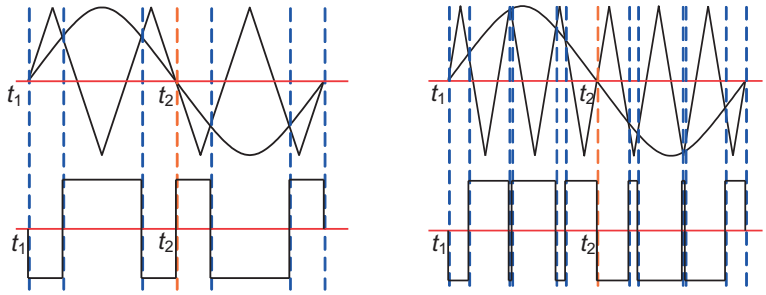

(a) (b)

Fig. 4. SPWM waveform: (a) when the carrier ratio is 3 odd times; (b) when the carrier ratio is 3 even times

Through the comparison and analysis, when the carrier ratio is 3 odd times, the output SPWM waveform is mirror symmetrical through comparing the wave of positive and negative half cycles, so the phase current has no even harmonics. When the carrier ratio is 3 even times, the output SPWM waveform is not mirror symmetrical, so the current includes even harmonics. Therefore, the switching frequency which is 3 odd times of the fundamental frequency is usually adopted.

Fig. 5 shows the phase current waveform of the generator when the switching frequency is 6 kHz, 21 kHz, and 45 kHz respectively. By calculating, the phase current RMS values are the same and about 133.0 A. From Fig. 5, it could be found that the phase currents have a lot of harmonics.

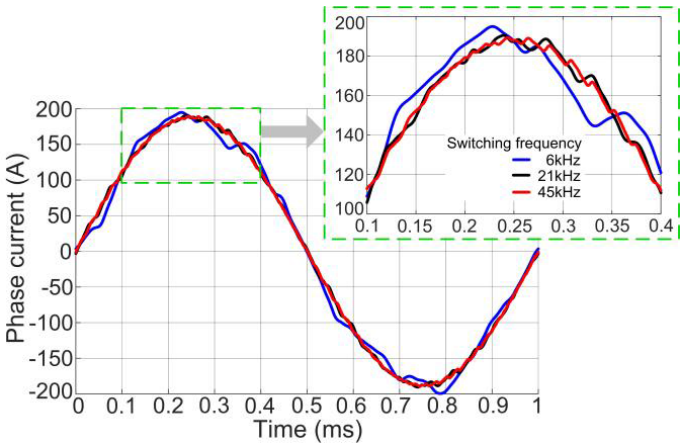

Fig. 5. Phase current in one cycle

By using the method of the Fourier decomposition, the harmonic contents in the generator are obtained and shown in Fig. 6 (harmonic currents, the amplitude of which is less than 0.15 A, are ignored).

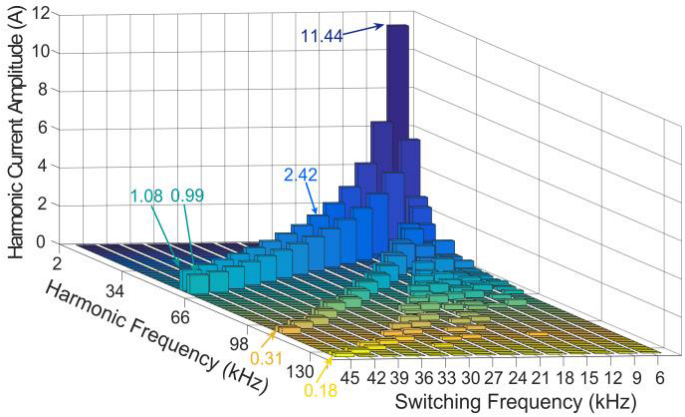

Fig. 6. Harmonic current frequency distribution of phase current

From Fig. 6, it becomes clear that the maximum value of the harmonic current is reduced with the increase of switching frequency. When the switching frequency is 6 kHz, the maximum value of the harmonic current reaches 11.44 A. When the switching frequency is 21 kHz, the maximum value of harmonic drops to 2.42 A, and the decline is 78.76%. When the switching frequency is 45 kHz, the maximum value of harmonic is only 1.08 A, and the decline is 90.6%. The frequency of the harmonic current is higher and higher. It can also be found that the content of the harmonic current is decreased with the increase of switching frequency. The number of harmonics is reduced from 27 to 6 when the switching frequency is from 6 kHz to 45 kHz, and all harmonics frequencies are higher. These higher harmonics will be filtered easily.

3.2. Total harmonic distortion of the phase current

The current total harmonic distortion (THD) represents the ratio of the current harmonic RMS value to the fundamental current RMS value. According to the above analysis of the harmonic content, the THD of the phase current under different switching frequency can be calculated by Formula (3) [6]:

$$\mathrm{THD} = \frac{\sqrt{\dfrac{1}{T}\displaystyle\int_T \left(\sum_{n-2}^{\infty} I_n \sin(n\omega t + \alpha_n)\right)^2 \mathrm{d}\,t}}{\sqrt{\dfrac{1}{T}\displaystyle\int_T (I_1 \sin(\omega t + \alpha_1))^2 \,\mathrm{d}\,t}} \times 100\%, \tag{3}$$

where: I_n is the RMS of the n-th harmonic current, I_1 is the RMS of the fundamental current.

It can be seen from Table 3 that the current THD is up to 7.30% when the switching frequency is 6 kHz. When the switching frequency is 21 kHz, the current THD is 1.81%, and drops by

5.49%. When the switching frequency is 45 kHz, the current THD is 0.84%, and drops by only 0.97% compared with 21 kHz. The relation between current THD and switching frequency is nonlinear. In other words, the effect of the increasing switching frequency on the reduction of the current THD becomes smaller and smaller.

Table 3. The THD of phase current under different switching frequency

Switching frequency (kHz)	**6**	**9**	**12**	**15**	**18**	**21**	**24**
Current THD (%)	7.30	4.45	3.24	2.56	2.12	1.81	1.58
The decrement (%)		2.85	1.21	0.68	0.44	0.31	0.23
Switching frequency (kHz)	**27**	**30**	**33**	**36**	**39**	**42**	**45**
Current THD (%)	1.40	1.25	1.14	1.05	0.97	0.89	0.84
The decrement (%)	0.18	0.15	0.11	0.09	0.08	0.08	0.05

4. The analysis of HSPMG losses

An HSPMG has the advantages of small size and large power density. However, it has the greater loss per volume comparing with the ordinary motor. Therefore, the output performance of the generator will be influenced seriously by too high generator temperature caused by generator loss, especially for the rotor. The cooling condition of the rotor is worse than the stator. Too high rotor temperature will cause the generation of the loss of the excitation fault, which can even threaten the safe operation of the generator. Therefore, the rotor eddy current loss is analyzed emphatically in this part.

During the analysis, the eddy current loss of the generator rotor is calculated in a cycle as follows (4) [4]:

$$P_{\text{eddy}} = \frac{1}{T}\int_T \sum_{i=1}^{k} J_e^2 \Delta_e \sigma_r^{-1} l_t \,\mathrm{d}\,t\,, \tag{4}$$

where J_e is the current density in each element (in A/m^2), Δ_e is the element area (in m^2), σ_r is the conductivity of the eddy current zone (in S/m), l_t is the rotor axial length (in m), P_{eddy} is the eddy current losses of the rotor (in W).

The curves of the rotor eddy current loss and its increase rate (comparing only with the fundamental current in the armature winding) under the influence of different switching frequency (including 6 kHz, 9 kHz, 12 kHz, . . . , 45 kHz) are shown in Fig. 7.

In Fig. 7, the increase rate represents the increase rate of the eddy current loss compared with the loss of the generator without harmonics. From Fig. 7, it becomes clear that with the increase of the switching frequency, the rotor eddy current loss is reduced, and the decline rate of the eddy current loss becomes smaller. When the switching frequency increases from 6 kHz to 21 kHz, the rotor eddy current loss decreases from 426.2 W to 350.8 W, and the decline rate (compared with the loss of the generator without harmonic) is 22.12%. When the switching frequency increases from 21 kHz to 45 kHz, the rotor eddy current loss decreases from 350.8 W to 344 W, the decline

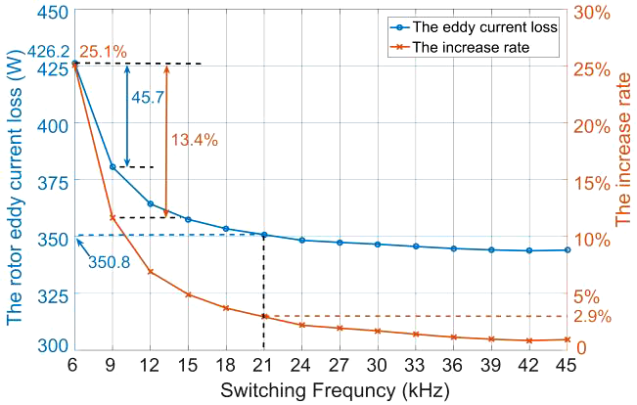

Fig. 7. The eddy current loss and the increase rate

rate is only 2%. The analysis above shows that the eddy current loss is approximately unchanged with the increase of switching frequency when the switching frequency is greater than 21 kHz.

The eddy current loss is proportional to the square of the eddy current density, and it is also proportional to the distribution range of the eddy current density. In order to reveal the change mechanism of the rotor eddy current loss, the eddy current density of the rotor is studied. Since the fundamental frequency is as high as 1 kHz or even higher, according to the skin effects, the eddy current density is mainly distributed on the rotor surface, and its value is decreased along the radial direction. When the eddy current density decays to $1/e$ (about 0.369) of the rotor surface value, this depth is described as the penetration depth. The penetration depth is calculated as following (5) [4]:

$$d = \sqrt{\frac{2}{\omega\mu\sigma}}, \tag{5}$$

where d is the penetration depth, ω is the angular frequency of the harmonic magnetic field, μ is the materials permeability, σ is the materials conductivity.

According to above Formula (5), the higher the harmonic magnetic field frequency is, the smaller the penetration depth is, and the eddy current density is more concentrated on the sleeve surface. Therefore, when the harmonic current amplitude is constant, the distribution range of the eddy current density will decrease with the increase of the harmonic magnetic field frequency.

Based on the finite element method, the rotor eddy current density of the generator under different switching frequency is calculated and analyzed. The eddy current density distribution of the rotor is shown in Fig. 8.

In order to compare the eddy current density during the analysis, the same scale is adopted. From Fig. 8, the eddy current is mainly in the rotor sleeve. With the increase of the switching frequency, the distribution range of the eddy current density decreases. Based on the result of the finite element analysis, it could be concluded that the maximum values of the eddy current density are 6.86×10^6 A/m^2, 5.95×10^6 A/m^2, 5.57×10^6 A/m^2, respectively, (see Fig. 8(a), (b), (c)). The maximum value of the eddy current density is decreased by 13.27% with the switching

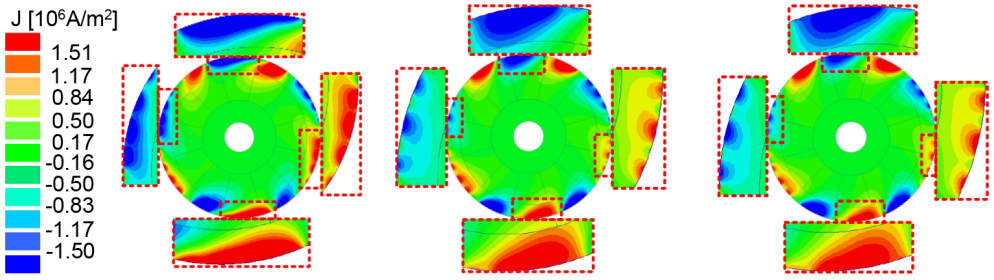

(a) (b) (c)

Fig. 8. The rotor eddy current density distribution: (a) when the switching frequency is 6 kHz; (b) when the switching frequency is 21 kHz; (c) when the switching frequency is 45 kHz

frequency increasing from 6 kHz to 21 kHz. Based on Formula (4), it could be verified that the eddy current loss also is decreased.

Through the analysis of the generator eddy current loss, it could be known that choosing 21 kHz switching frequency can reduce the rotor eddy current loss of the generator effectively by 22.12%, and make sure that the switching loss of the converter is within a reasonable range. This way, the loss of the entire system would be reduced.

5. The analysis of HSPMG torque

The torque ripple directly reflects the stability of generator operation. An excessive torque ripple not only results in vibration and noise in the generator operation, but also threatens the safe and stable running of the generator. It may even cause the fault of the whole distributed power generation system. Therefore, it is very important to be sure about the analysis of the generator torque.

In this part, the influence of the rectifier switching frequency on the torque of an HSPMG is analyzed. Based on the analysis of harmonic current contents of the system under different work conditions, by using the time stepping finite element analysis model, the average torque, the maximum torque and the minimum torque of the generator are obtained. During the analysis, the torque is the electromagnetic torque.

In order to describe the change of the torque ripple accurately, the torque ripple was defined as Formula (6) [20]:

$$\delta = \frac{\sqrt{\sum_{1}^{n}(T_{i\max} - T_{\text{avg}})^2 + \sum_{1}^{n}(T_{i\min} - T_{\text{avg}})^2}}{nT_{\text{avg}}}, \tag{6}$$

where δ is the torque ripple, $T_{i\max}$, $T_{i\min}$ are the maximum and minimum of torque in some cycles, T_{avg} is the average torque, n is the number of cycles.

The torque and torque ripple are shown in Fig. 9.

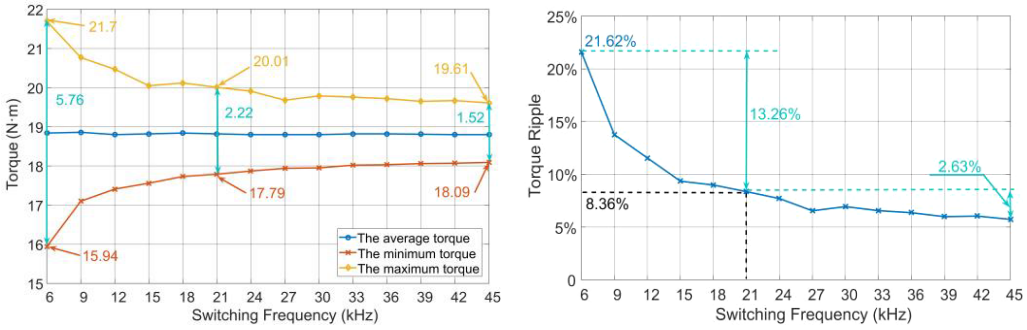

(a) (b)

Fig. 9. Torque of the generator with different switching frequency: (a) the torque; (b) the torque ripple

In order to ease to analysis and understanding, the absolute value of torque is used in the analysis of HSPMG torque.

Through the analysis of Fig. 9(a), the conclusion can be drawn that the average torque of the generator is constant (about –18.81 N·m). But the maximum torque of the generator is decreased and the minimum torque is increased with the switching frequency increasing. So the torque ripple range is reduced.

Based on the analysis of Fig. 9, the torque ripple range is decreased with the switching frequency increasing. The torque ripple range decreases from 5.76 N·m to 2.22 N·m when the switching frequency increases from 6 kHz to 21 kHz, and the drop is 61.46%. However, when the switching frequency exceeds 21 kHz, the decrement of the torque ripple range becomes smaller. The variation trend of the torque ripple is consistent with the variation trend of the torque ripple range.

The torque ripple is 21.62% when the switching frequency is 6 kHz. The torque ripple is 8.36% when the switching frequency is 21 kHz, and the drop is 13.26%. When the switching frequency is 45 kHz, the torque ripple is 5.73%, so the drop is only 2.63%. Through the above analysis, it could be obtained that the torque ripple can be reduced effectively and the stability of the generator operation can be improved when the switching frequency is 21 kHz. When the switching frequency exceeds 21 kHz, the generator torque ripple is reduced, but the effect of the weakening torque ripple becomes smaller and smaller.

6. Conclusions

In this paper, an HSPMG driven by a micro gas turbine is the object of study. The effects of the switching frequency on the system harmonic current content, losses and torque of the generator in the distributed generation system are studied through the indirect field-circuit coupling method between the finite element model and the state-space model, and this method can save a lot of time compared to the direct coupling method. The following conclusions are drawn.

1. The phase current RMS value is unchanged and about 133.0 A. The current THD is decreased with the increase of the switching frequency, but its drop becomes smaller and smaller. When the switching frequency increases from 6 kHz to 21 kHz, the current THD drops by 5.49%. When the switching frequency increases from 21 kHz to 45 kHz, the current THD drops by only 0.97%.
2. The rotor eddy current loss reduces from 426.2 W to 350.8 W when the switching frequency increases from 6 kHz to 21 kHz. However, when the switching frequency increases from 21 kHz to 45 kHz, the eddy current loss reduces only from 350.8 W to 344 W. The rotor eddy current loss is decreased with the increase of the switching frequency. But the decline rate of the eddy current losses becomes smaller when the switching frequency exceeds 21 kHz.
3. The torque ripple can be reduced more effectively when the switching frequency is properly increased. When the switching frequency is increased excessively, the effect of weakening torque ripple becomes smaller and smaller. Compared with a torque ripple of 6 kHz switching frequency, the torque ripple decreases by 13.26% when the switching frequency increases to 21 kHz. When the switching frequency increases to 45 kHz, the torque ripple decreases by only 2.63%.
4. Through the analysis of this paper, the 21 kHz switching frequency of the studied distributed power generation system is more appropriate. Not only can it improve operational performance and reduce the loss of an HSPMG with a rectifier, but can also reduce unnecessary rectifier switching losses.

Acknowledgements

This work was supported in part by the National Natural Science Foundation of China under Grant 51507156, in part by the University Key Scientific Research Programs of Henan province under Grant 17A470005, in part by the Doctoral Program of Zhengzhou University of Light Industry under Grant 2014BSJJ042, in part by the Major Science and Technology Special Projects of Henan Province under Grant 161100211600, in part by the Scientific and Technological Projects of Zhengzhou under Grant 20150442, and in the part by the Graduate Scientific and Technology Innovation Foundation of Zhengzhou University of Light Industry under Grant 2017011.

References

[1] Weili Li, Hongbo Qiu, Xiaochen Zhang, Ran Yi, *Influence of Copper Plating on Electromagnetic and Temperature Fields in a High-Speed Permanent-Magnet Generator*, IEEE Transactions on Magnetics, vol. 48, no. 8, pp. 2247–2253 (2012).

[2] Patel Ashish, Arya Sabha Raj, *Distributed power generation system using PMSG with power quality features*, Proceedings of International Conference on Next Generation Intelligent Systems, Kottayam, pp. 1–8 (2017).

[3] Zhang Xiaochen, Li Weili, Cheng Shukang, Kou Baoquan, Geng Jiamin, Wang Jing, *Thermal Analysis of High Speed PM Generator used for distributed generation system*, Proceedings of International Conference on Power System Technology, Hangzhou, pp. 1–7 (2010).

[4] Li Weili, Qiu Hongbo, Zhang Xiaochen, Cao Junci, Yi, Ran, *Analyses on Electromagnetic and Temperature Fields of Superhigh-Speed Permanent-Magnet Generator with Different Sleeve Materials*, IEEE Transactions on Industrial Electronics, vol. 61, no. 6, pp. 3056–3063 (2014).

[5] Qiu Hongbo, Tang Bingxia, Yu Wenfei, Yuan Shuai, Wu Jie, Yang Cunxiang, Cui Guangzhao, *Analysis of the super high-speed permanent magnet generator under unbalanced load condition*, IET Electric Power Applications, vol. 11, no. 8, pp. 1492–1498 (2017).

[6] Hongbo Qiu, Ran Yi, Weili Li, Nan Jin, *Influence of Rectifiers on High-Speed Permanent Magnet Generator Electromagnetic and Temperature Fields in Distributed Power Generation Systems*, IEEE Transactions on Energy Conversion, vol. 30, no. 2, pp. 655–662 (2015).

[7] Li Jing, Zhang Xiaochen, Zhang He, Huang Xiaoyan, Gerada Chris, Galea Michael, *Control Integrated Studies on High Speed Permanent Magnetic Generators System*, IEEE Transactions on Magnetics, vol. 51, no. 11 (2015), DOI: 10.1109/TMAG.2015.2451102.

[8] Van Der Geest M., Polinder H., Ferreira J.A., *Influence of PWM switching frequency on the losses in PM machines*, Proceedings of International Conference on Electrical Machines, Berlin, pp. 1243–1247 (2014).

[9] Krings A., Soulard J., Wallmark O., *Influence of PWM Switching Frequency and Modulation Index on the Iron Losses and Performance of Slot-less Permanent Magnet Motors*, Proceedings of International Conference on Electrical Machines and Systems, Busan, pp. 474–479 (2013).

[10] Krings A., Soulard J., Wallmark O., *PWM Influence on the Iron Losses and Characteristics of a Slotless Permanent-Magnet Motor with SiFe and NiFe Stator Cores*, IEEE Transactions on Industry Applications, vol. 51, no. 2, pp. 1475–1484 (2015).

[11] Ding Shuye, Li Hailing, *Analysis of Iron Loss for Permanent Magnet Synchronous Motor Driven by PWM*, Proceedings of IEEE Vehicle Power and Propulsion Conference, Hangzhou, pp. 1–6 (2016).

[12] Boglietti A., Ferraris P., Lazzari M., Pastorelli M., *Change of the iron losses with the switching supply frequency in soft magnetic materials supplied by PWM inverter*, IEEE Transactions on Magnetics, vol. 31, no. 6, pp. 4250–4252 (1995).

[13] Merdzan M., Paulides J.J.H., Borisavljevic A., Lomonova E.A., *The influence of the inverter switching frequency on rotor losses in high-speed permanent magnet machines: an experimental study*, Proceedings of IEEE International Electric Machines & Drives Conference, Coeur d'Alene, pp. 1628–1633 (2015).

[14] Nobuhito Kometani, Yukinori Inoue, Shigeo Morimoto, Masayuki Sanada, *Calculation Reduction Method for Ultra-High Speed PMSM Drive System Based on Direct Torque Control in M-T Frame*, Proceedings of 19th International Conference on Electrical Machines and Systems, Chiba, pp. 1–6 (2016).

[15] Merdzan M., Paulides J.J.H., Lomonova E.A., *Comparative Analysis of Rotor Losses in High-Speed Permanent Magnet Machines with Different Winding Configurations Considering the Influence of the Inverter PWM*, Proceedings of Tenth International Conference on Ecological Vehicles and Renewable Energies, Monte Carlo, pp. 1–8 (2015).

[16] Yingjie Li, Di Han, Bulent Sarlioglu, *Design of High-Speed Machines Using Silicon-Carbide Based Inverters*, Proceedings of IEEE Energy Conversion Congress and Exposition, Montreal, pp. 3895–3900 (2015).

[17] Zhou P., Lin D., Fu W.N., Ionescu B., Cendes Z.J., *A general cosimulation approach for coupled field-circuit problems*, IEEE Transactions on Magnetics, vol. 42, no. 4, pp. 1051–1054 (2006).

[18] Zhang Xiaochen, Li Weili, Zhang He, Gerada Chris, Galea Michael, Li Jing, *Topology investigation on high speed PM generator with back wound windings*, Proceedings of IEEE 25th International Symposium on Industrial Electronics, Santa Clara, pp. 234–239 (2016).

[19] Nazempour A., Khaburi D.A., *Simulation of the PWM rectifier connected to a high frequency power sources*, Proceedings of 1st Power Electronic & Drive Systems & Technologies Conference, pp. 169–174, Tehran, Iran (2010).

[20] Qiu Hongbo, Yu Wenfei, Li Yonghui, Yang Cunxiang, *Research on the influence of driving harmonic on electromagnetic field and temperature field of permanent magnet synchronous motor*, Archives of Electrical Engineering, vol. 66, no. 2, pp. 295–312 (2017).